

A Diff-Attention Aware State Space Fusion Model for Remote Sensing Classification

Wenping Ma, *Senior Member, IEEE*, Boyou Xue, Mengru Ma, Chuang Chen, Hekai Zhang, Hao Zhu, *Member, IEEE*

Abstract—Multispectral (MS) and panchromatic (PAN) images describe the same land surface, so these images not only have their own advantages, but also have a lot of similar information. In order to separate these similar information and their respective advantages, reduce the feature redundancy in the fusion stage. This paper introduces a diff-attention aware state space fusion model (DAS²F-Model) for multimodal remote sensing image classification. Based on the selective state space model, a cross-modal diff-attention module (CMDA-Module) is designed to extract and separate the common features and their respective dominant features of MS and PAN images. Among this, space preserving visual mamba (SPVM) retains image spatial features and captures local features by optimizing visual mamba's input reasonably. Considering that features in the fusion stage will have large semantic differences after feature separation and simple fusion operations struggle to effectively integrate these significantly different features, an attention-aware linear fusion module (AALF-Module) is proposed. It performs pixel-wise linear fusion by calculating influence coefficients. This mechanism can fuse features with large semantic differences while keeping the feature size unchanged. Empirical evaluations indicate that the presented method achieves better results than alternative approaches. The relevant code can be found at: <https://github.com/AVKSKVL/DAS-F-Model>.

Index Terms—Mamba, multimodal, feature separation, feature fusion, fusion classification

I. INTRODUCTION

In recent years, enhancing remote sensing image classification accuracy through multisource fusion has become a key area of research. With the rapid advancement of satellite technology, there is an increasing demand for high-quality, high-resolution multispectral remote sensing images [1], [2]. Modern satellites are capable of capturing panchromatic (PAN) images with very high spatial resolution, along with multispectral (MS) images [3], [4] that provide abundant spectral information. However, the resolution of MS images is obviously lower than that of PAN images, although they contain more spectral details [5]. The combination of these complementary features enables effective fusion and classification for various practical applications, such as deforestation monitoring [6], urban planning [7], [8], precision agriculture [9], land-cover classification [10], [11], and mineral exploration [12], [13].

In remote sensing, multisource classification algorithms are primarily categorized into two types: traditional methods and deep learning-based algorithms [14]–[17].

The authors are with the Key Laboratory of Intelligent Perception and Image Understanding of Ministry of Education, International Research Center for Intelligent Perception and Computation, School of Artificial Intelligence, Xidian University, Xi'an 710071, China (Corresponding authors: Mengru Ma, e-mail: mengrumalearn@163.com).

A common traditional approach involves applying pan-sharpening [18]–[20] to MS images before classification. These algorithms require appropriate pan-sharpening techniques usually, such as component substitution (CS) [21] and multi-resolution analysis (MRA) [22]. Another traditional approach involves feature fusion followed by classification, where features are extracted separately from PAN and MS images. Jia et al. [23] employed gabor filters to process the spectral-spatial domain, subsequently proposing an algorithm that fuses spectral-spatial features using Gabor surface representations based on this framework. Hedhli et al. [24] proposed two classification methods for remote sensing images with different spatial resolutions, based on hierarchical Markov random fields. However, these conventional methods often rely on handcrafted features and manually designed fusion rules, which may not effectively capture the complex relationships between multi-modal data.

In recent years, with the rapid advancement of deep learning theory and hardware resources, significant progress has been made in deep learning-based multimodal fusion classification algorithms. Among these, convolutional neural network (CNN) and Transformer architectures have emerged as predominant research directions. The CNN framework enhances classification precision by leveraging its exceptional capacity for localized feature capture and sophisticated multi-scale integration techniques. Meanwhile, the Transformer paradigm employs its distinctive attention mechanism [25]–[27] to effectively model long-range contextual relationships within sequential data.

Based on the CNN method, Ma et al. [28] introduced the interactive spatial-spectral perception network (ISSP-Net). This network addressed the challenge of optimizing the complementary information between PAN and MS images by enhancing spatial location interaction and integrating multi-scale context through pixel-guided spatial enhancement. Lu et al. [29] proposed coupled adversarial learning for classification (CALC), which learned more discriminative fusion features thanks to an optimally designed joint loss function that included both unsupervised adversarial and supervised classification losses. Zhu et al. [30] proposed a multi-scale frequency fusion network. A multi-scale frequency feature extractor based on ConvGRU is used to obtain more comprehensive scale-enhanced texture features. Zhao et al. [31] designed a scale-aware neighborhood correlation feature network (SNCF-Net). By constructing a scale-aware attention mechanism, the utilization of features is effectively improved. However, their ability to capture global information was somewhat limited, which restricted the model's capacity to understand

and analyze complex scenes.

Based on the Transformer method, Zhu et al. [32] proposed an adaptive spatial and channel attention module to enhance the own features of PAN and MS images through progressive fusion. Xu et al. [33] proposed a dual-stream transformer based on diff-attention (DSTD-Net), which extracted the advantageous features and common essential features by using self-attention and co-attention, reduced the essential redundancy in the advantageous features by diff-attention enhancement. Roy et al. [34] proposed a novel multimodal fusion transformer network (MFT). This approach employs multi-head cross-patch attention to learn distinctive representations in simplified and hierarchical feature spaces. The S²ENet [35] included a spatial enhancement module (SAEM) and a spectral enhancement module (SEEM) to enhance spatial and spectral features used LiDAR and HS images, respectively. However, it is worth noting that although transformer-based fusion classification models showed great potential in feature extraction and fusion, their high computational cost and optimization difficulty were also challenges that cannot be ignored.

Although the above work has achieved considerable results, there are still many problems to be solved:

(1) From text to visual domain, simply replacing one-dimensional convolution with deep convolution will lead to the convolution objects are not adjacent in the physical space, thus introducing useless spatial noise, which is not conducive to the retention and extraction of spatial information.

(2) There are a large number of similar redundant features in MS and PAN images. This results in important information that plays a key role in downstream tasks being submerged in these redundancies, seriously affecting the subsequent classification performance.

(3) When fusing multimodal features, simple fusion operations are difficult to effectively fuse features with large semantic differences. Even if gating based methods [33] are applied, the huge difference between features is still difficult to effectively compensate.

In order to solve the above problems, this paper proposes a diff-attention aware state space fusion model (DAS²F-Model) for remote sensing classification. The main contributions are as follows:

(1) For the preservation of spatial information, a space preserving visual mamba (SPVM) is proposed. By reasonably adjusting the input features of visual mamba, the deep convolutional layer can effectively obtain the local features of images, which promotes the effective combination of the state space model and the traditional visual model.

(2) To solve the problem of large redundancy in MS and PAN feature fusion, a cross-modal diff-attention module (CMDA-Module) is proposed. This module achieves the separation of common and dominant features of MS and PAN image by exchanging a series of matrices in the state space model. This greatly reduce the redundancy of fusion features, which enables the DAS²F-Model to pay more attention to more important key information in subsequent classification and improves the performance of classification.

(3) For the difficult to fuse features with large semantic differences effectively, this paper proposes an attention-aware

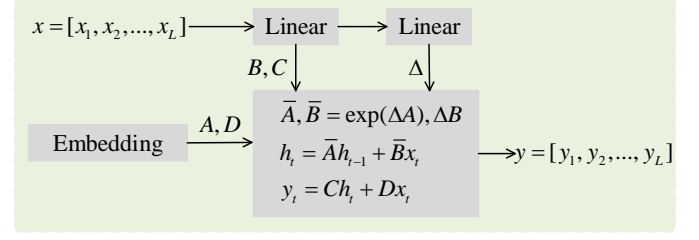


Fig. 1: Linear-Time Sequence Modeling with Selective State Spaces (Mamba)

linear fusion module (AALF-Module). The module performs pixel-wise linear fusion by dynamically calculating influence coefficients, allowing one modality to guide the fusion process of the other at each spatial location. This mechanism can fuse features with large semantic differences while keeping the feature size unchanged.

The present paper is structured as follows: Section II explains the relevant work, Section III introduces the DAS²F-Model algorithm comprehensively, Section IV verifies the effectiveness of the DAS²F-Model through a series of rigorous experiments, as well as Section V is the conclusion and future development direction of this paper.

II. RELATED WORK

This section will introduce two tasks related to our method in detail. They are the state space model and multimodal fusion classification.

A. State Space Model

State space model (SSM) is a mathematical model used to describe dynamic systems. It represents the state of the system as a vector that evolves over time. In the structured state space sequence model (S4), the transformation from input $x(t) \in \mathbb{R}$ to output $y(t) \in \mathbb{R}$ is mediated by an N-dimensional hidden state space $h(t) \in \mathbb{R}^N$, as described by the following ordinary differential equation:

$$\begin{aligned} \bar{A} &= \exp(\Delta A), \\ \bar{B} &= (\Delta A)^{-1}(\exp(\Delta A) - \mathbf{I}) \cdot \Delta B, \end{aligned} \quad (1)$$

$$\begin{aligned} h_t &= \bar{A} h_{t-1} + \bar{B} x_t, \\ y_t &= C h_t + D x_t, \end{aligned} \quad (2)$$

where, Δ is a learnable parameter used for the discretized data continuation, $A \in \mathbb{R}^{N \times N}$ is the state transition matrix, $B \in \mathbb{R}^{N \times 1}$ and $C \in \mathbb{R}^{1 \times N}$ are the matrices responsible for transforming inputs into states and states into outputs, respectively. Although the S4 model has linear computational complexity, it is difficult to capture the sequence context because the parameter matrix is a fixed constant.

On this basis, S6 (Mamba [36]) model came into being. By introducing a selective mechanism (see Fig.1), Mamba enables the model to dynamically adjust the state transition and observation process, so as to better adapt to different input characteristics and task requirements. Specifically, Mamba

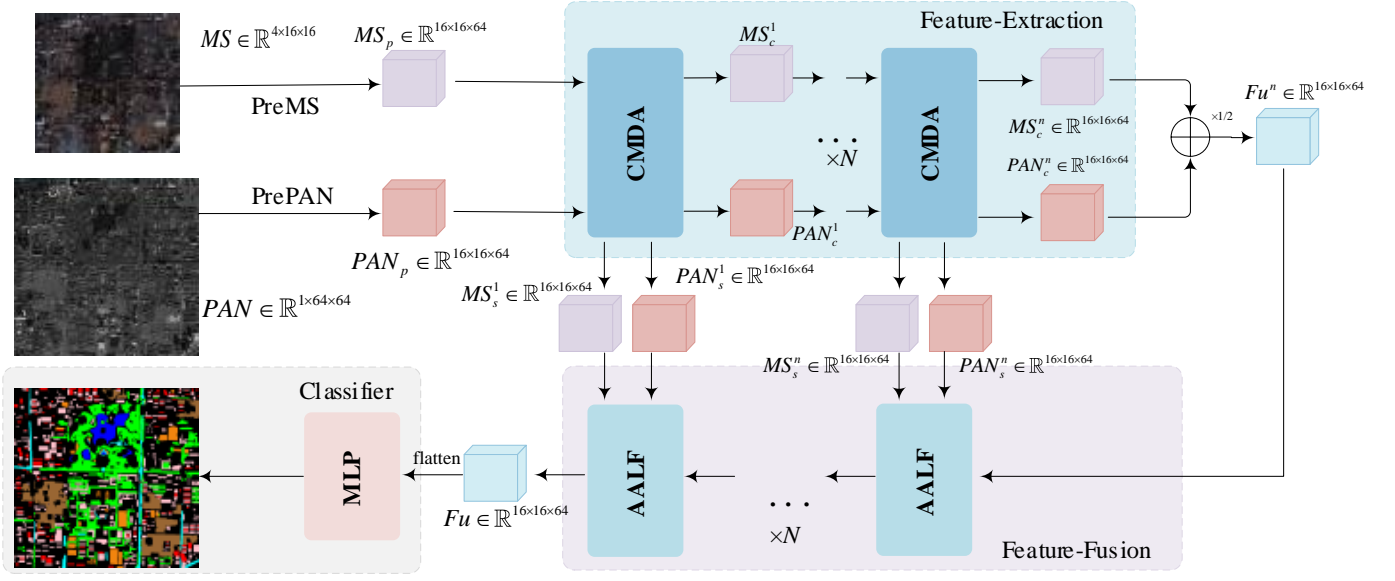


Fig. 2: Diff-Attention Aware State Space Fusion Model (DAS²F-Model). PreMS and PrePAN denote the preprocessing process for MS and PAN, respectively. CMDA-Module means cross-modal diff-attention module. AALF-Module is attention-aware linear fusion module. \oplus means element-wise sum. N represents the number of CMDA-Module and AALF-Module.

gets the parameter matrix B , C , Δ based on the input $x \in \mathbb{R}^{B \times L \times D}$:

$$\begin{aligned} B, C, \Delta_1 &= \text{Linear}(x), \\ \Delta &= \text{Linear}(\Delta_1), \end{aligned} \quad (3)$$

where $\Delta \in \mathbb{R}^{B \times L \times D}$, $B \in \mathbb{R}^{B \times L \times N}$ and $C \in \mathbb{R}^{B \times L \times N}$. Furthermore, this model has been applied in the field of multimodal fusion classification [37].

B. Multimodal fusion classification

multimodal fusion classification is an emerging research field that focuses on integrating heterogeneous data from various sensors or sources. By leveraging the synergy and complementarity of these multimodal data, this approach significantly enhances both the accuracy and robustness of remote sensing image classification.

For instance, Liu et al. [38] introduced the cross-resolution hidden layer feature fusion (CRHFF) method to better model objects using multimodal representations. By integrating multi-scale features from MS and PAN images, their approach significantly boosts classification performance. Gao et al. [39] proposed a deep feature interaction network (DFINet), which is able to extract the autocorrelation and cross-correlation of multisource features. At the same time, it is optimized by coordinating the consistency loss, discrimination loss and classification loss. Wang et al. [40] proposed a nearest neighbor based contrastive learning network (NNCNet), which makes full use of a large amount of unlabeled data to learn discriminative feature representations, effectively reducing the heterogeneous gap caused by the inconsistent distribution of multisource data.

However, none of the above methods take into account that multimodal features may contain substantial similar redundant information, thereby failing to enable the model to focus on

the critical information that determines the performance of classification tasks.

III. METHODOLOGY

In order to effectively separate the common essential features and their respective dominant features of MS and PAN images, as well as fuse the features with large semantic differences, we propose diff-attention aware state space fusion model (DAS²F-Model: Sec.III-A, see Fig. 2) for multimodal remote sensing image classification. The model consists of three modules: the space preserving visual mamba (SPVM: Sec.III-B, see Fig. 3), the cross-modal diff-attention module (CMDA-Module: Sec.III-C, see Fig. 4) and the attention-aware linear fusion module (AALF-Module: Sec.III-D, see Fig. 5), where the SPVM is included in the CMDA-Module.

A. Diff-Attention Aware State Space Fusion Model (DAS²F-Model)

Multispectral images ($MS \in \mathbb{R}^{4 \times 16 \times 16}$) provide rich spectral data by capturing radiometric information of multiple spectral bands, which makes the identification and analysis of types of ground objects more accurate. Panchromatic images ($PAN \in \mathbb{R}^{1 \times 64 \times 64}$) focus on high-resolution imaging of a single visible band, revealing texture and structural features of the surface with extremely high pixel detail.

In this paper, MS and PAN images are first processed by up-sampling and convolution operations to obtain MS_{up} and PAN_R of the same size ($MS_{up} \in \mathbb{R}^{4 \times 64 \times 64}$, $PAN_R \in \mathbb{R}^{4 \times 64 \times 64}$), respectively. This is followed by patching MS and PAN images to obtain $MS_p \in \mathbb{R}^{16 \times 16 \times 64}$ and $PAN_p \in \mathbb{R}^{16 \times 16 \times 64}$. In Fig.2, these two steps are combined into a pre-processing block:

$$\begin{aligned} MS_p &= \text{PreMS}(MS), \\ PAN_p &= \text{PrePAN}(PAN). \end{aligned} \quad (4)$$

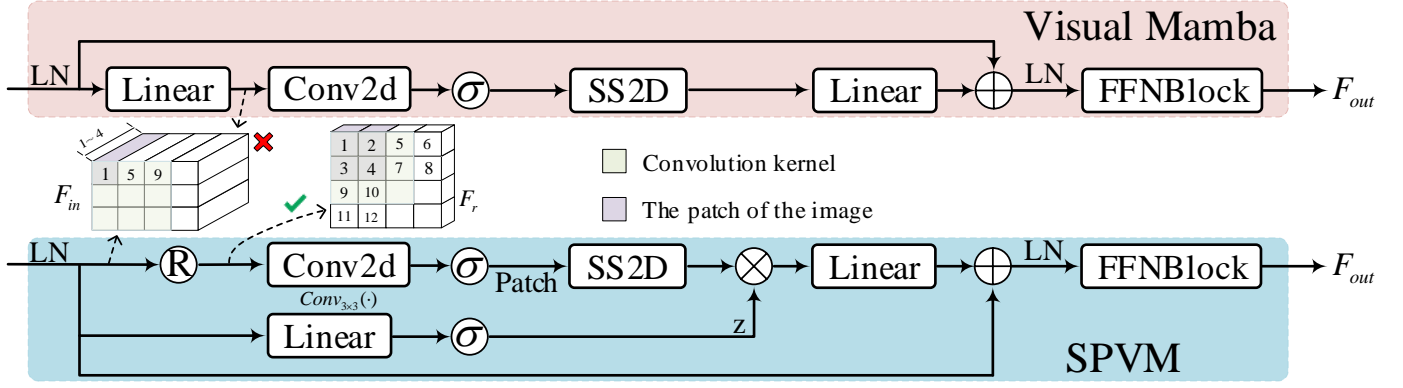


Fig. 3: Comparison between Space Preserving Visual Mamba (SPVM) and Visual mamba. \otimes means element-wise multiplication. R represents the reshape operation, σ represents the SiLU activation function.

Then, the common essential features and their respective dominant features of MS and PAN images are extracted and separated through the CMDA-Module, and the output MS_c^1, PAN_c^1 and MS_s^1, PAN_s^1 ($\mathbb{R}^{16 \times 16 \times 64}$) is obtained:

$$MS_c^1, MS_s^1, PAN_c^1, PAN_s^1 = \text{CMDA}^1(MS_p, PAN_p), \quad (5)$$

where MS_c^1 and PAN_c^1 are the common shallow essential features of MS and PAN images, MS_s^1 and PAN_s^1 are the shallow dominant features of MS and PAN images respectively. $\text{CMDA}^1(\cdot)$ represents the first cross-modal diff-attention module.

The respective shallow dominant features MS_s^1 and PAN_s^1 are fused in subsequent AALF-Module. The common essential features MS_c^1 and PAN_c^1 are then fed into the subsequent CMDA-Module for further extraction and separation, ultimately produces their deeper dominant features and the common essential features MS_c^n, PAN_c^n . Considering that MS_c^n and PAN_c^n are sufficiently similar, the preliminary fusion features $Fu^n \in \mathbb{R}^{16 \times 16 \times 64}$ are obtained by averaging MS_c^n and PAN_c^n :

$$MS_c^i, MS_s^i, PAN_c^i, PAN_s^i = \text{CMDA}^i(MS_c^{i-1}, PAN_c^{i-1}), \quad (6)$$

$$Fu^n = (MS_c^n + PAN_c^n)/2. \quad (7)$$

Next, through a series of AALF-Module, Fu^n sequentially fuse the dominant features of MS and PAN images to obtain the non-redundant multimodal fusion features $Fu \in \mathbb{R}^{16 \times 16 \times 64}$. Finally, it is directly entered into a multi-layer perceptron (MLP) for subsequent classification:

$$L = -\frac{1}{N} \sum_{i=1}^N \sum_{j=1}^C y_{ij} \log(\text{MLP}(Fu))_{ij}. \quad (8)$$

Among them, N is the number of samples in the batch, C is the number of labeled categories in the ground truth, y_{ij} indicates whether the i th sample belongs to the j th class or not, and its value is 0 or 1. $(M_{lp}(Fu))_{ij}$ denotes the probability that the i th sample belongs to the j th class.

The DAS²F-Model cleverly separates the common and dominant features of MS and PAN images through the cross-modal diff-attention mechanism. It is particularly worth mentioning

that the attention-aware linear fusion module effectively incorporates features with large semantic differences by using influence coefficients to guide pixel-by-pixel fusion, which further improves the robustness and generalization ability of the model.

B. Space Preserving Visual Mamba (SPVM)

Visual mamba replaces Mamba's one-dimensional convolutional layer with deep convolution (DWConv) to adapt to image. However, the parts of the feature map that are convolved are not adjacent in the physical space, which makes the deep convolution not only fail to obtain local features, but also introduce useless spatial noise. Therefore, we design the space preserving visual mamba (SPVM, see Fig.3), which can capture the local context relationship between independent tokens while obtaining the local features of the data well.

(1) Obtain local and context features between tokens. In order to obtain local features, this paper reshapes the feature map before convolutional layer. Specifically, first, divide each image patch of F_{in} along the channel axis, that is, $\mathbb{R}^{B \times 16 \times 16 \times (4 \times 4 \times 4)}$. Then, reassemble the separated patches back to their initial spatial locations, that is, $\mathbb{R}^{B \times (16 \times 4) \times (16 \times 4) \times 4}$. Finally, reshape the feature map back to its 3D form, that is, $F_r \in \mathbb{R}^{B \times 4 \times 64 \times 64}$. The feature map with local features can be obtained by processing F_r with a convolutional neural network, which can also capture the local context relationship between adjacent tokens, so that each token is no longer independent without interactive. The feature maps are then converted back into sequences $F_p \in \mathbb{R}^{B \times 16 \times 16 \times 64}$ via re-patching to facilitate subsequent operations. The specific process is as follows:

$$F_r = \text{Reshape}(F_{in}), \quad (9)$$

$$F_p = \text{Conv}_p(\text{Conv}_{3 \times 3}(F_r)). \quad (10)$$

Among them, $\text{Conv}_p(\cdot)$ denotes the convolutional neural network responsible for re-patching.

(2) Capture global features. Due to the sequential nature of the mamba scan operation, it is not suitable for visual data, visual mamba proposed the 2D selective scanning (SS2D) module to solve this problem. First, SS2D is retained in this paper

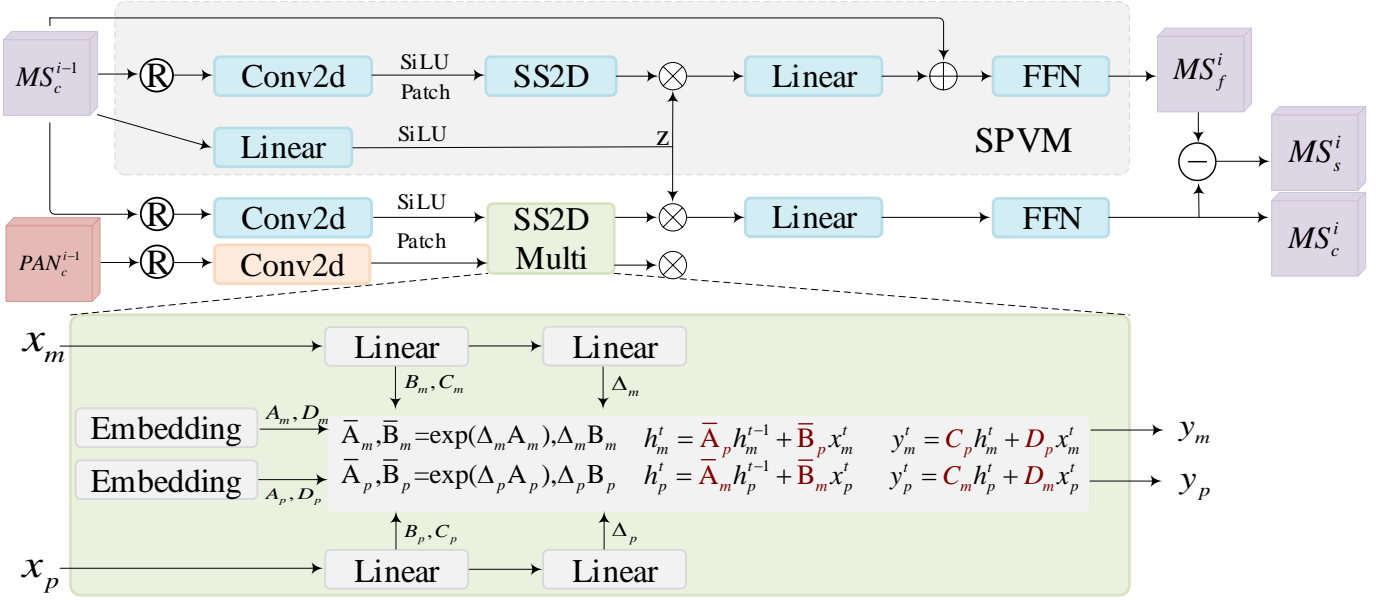


Fig. 4: Cross-Modal Diff-Attention Module (CMDA-Module). \ominus is element-wise subtraction.

to process $F_p \in \mathbb{R}^{B \times 16 \times 16 \times 64}$. Then $F_{out} \in \mathbb{R}^{B \times 16 \times 16 \times 64}$ with global and local features is acquired by linear mapping (linear) and feed-forward neural network (FFN). In addition, this paper also retains the gated MLP branch z that is deleted by visual mamba but exists in mamba, allowing the model to focus more on key information that has a greater impact on downstream tasks. The specific process is as follows:

$$z = \text{SiLU}(\text{Linear}_z(F_{in})), \quad (11)$$

$$F_{out} = \text{FFN}(\text{Linear}_{out}(\text{SS2D}(F_p) \times z)). \quad (12)$$

Among them, $\text{Linear}_z(\cdot)$ represents the gated MLP, $z \in \mathbb{R}^{B \times 16 \times 16 \times 64}$ represents the gating coefficient, $\text{Linear}_{out}(\cdot)$ is the output linear mapping layer, and $\text{FFN}(\cdot)$ is a feed forward neural network with one hidden layer.

The SPVM appropriately adjusts the input dimension to preserve the spatial features of the images. It should be noted that traditional computer vision methods often require data to maintain 3D shape (B,C,H,W), while state space model, as a sequence model, requires input data to maintain sequence state (B,L,D). This makes it difficult to combine the advantages of traditional vision methods with state space models. In this paper, our SPVM deletes the linear mapping layer existing in Mamba and visual mamba, so that input can be freely reshaped and patched, which combine with the traditional vision method more flexibly, creating more possibilities for the deep combination of sequence model and visual model.

C. Cross-Modal Diff-Attention Module (CMDA-Module)

MS and PAN images are remote sensing data of different modalities in the same scene, which means that they have a lot of semantic redundant information. To this end, we present a cross-modal diff-attention module (CMDA-Module) to reduce redundant information and improve the feature representation ability. The detailed implementation is illustrated in Fig.4. In

the figure, only the specific design details of the MS branch are shown, and the design details of the PAN branch are similar to the MS branch.

(1) Intra-modal feature extraction. The current level's intra-modal features MS_f^i are generated by applying the aforementioned SPVM approach to process the level's input features MS_c^{i-1} , specifically:

$$MS_f^i = \text{SPVM}(MS_c^{i-1}). \quad (13)$$

(2) Inter-modal essential feature extraction. In the process of feature extraction, the state space model generates a sequence of intermediate matrices for different data. These matrices focus on different stages in the feature extraction process, and they can guide network to generate the most critical features of the modality.

From a signal processing point of view, the response between signals with similar feature distributions is stronger than that between signals with different feature distributions. That is, the response of the common part between the multimodal features is stronger than the response of the respective advantage part.

Therefore, this paper utilizes the intermediate matrices generated by the SSM during the feature extraction process of PAN images to process the features of MS images. Specifically:

$$\begin{aligned} h_m^t &= \bar{A}_p h_m^{t-1} + \bar{B}_p x_m^t, \\ y_m^t &= C_p h_m^t + D_p x_m^t, \end{aligned} \quad (14)$$

where, A_p, B_p, C_p and D_p represent the intermediate matrices generated during the SSM processing of the PAN image. x_m^t and y_m^t denote the input and output features of the MS image, respectively. During this process, features in the MS image that are similar to those in the PAN image are preserved, while dissimilar features are suppressed. This operation replaces the SS2D block in SPVM, while the remaining feature processing blocks remain identical to those in SPVM. The

processed result is the common features of the MS image MS_c^i . Specifically:

$$MS_c^i = \text{FFN}(\text{Linear}(\psi(\text{Conv}(\text{R}(MS_c^{i-1})) \times z))), \quad (15)$$

where, $\text{R}(\cdot)$ stands for the reshape operation and $\psi(\cdot)$ refers to the SS2DMulti block.

(3) Dominant feature acquisition. Intra-modal feature MS_f^i and PAN_f^i contains all the information of its corresponding branch. By subtracting these inter-modal common essential features from the intra-modal features of the branch, the dominant features of the MS and PAN modality $MS_s^i \in \mathbb{R}^{16 \times 16 \times 64}$ and $PAN_s^i \in \mathbb{R}^{16 \times 16 \times 64}$ can be obtained respectively, specifically:

$$MS_s^i = MS_f^i - MS_c^i, \quad (16)$$

$$PAN_s^i = PAN_f^i - PAN_c^i. \quad (17)$$

The CMDA-Module can separated the common essential features and respective dominant features of MS and PAN images well, which greatly reduces the redundant information of subsequent fusion features and improves the robustness and generalization ability of the model.

D. Attention-Aware Linear Fusion Module (AALF-Module)

Considering that the features to be fused are the respective advantages of MS and PAN and their common essential features, Thus there are considerable differences. This paper proposes an attention-aware linear fusion module (AALF-Module). This module can effectively fuse features with large semantic differences while keeping the size of the fusion result unchanged, see Fig.5 for details.

(1) Generate attention coefficient matrix G. For the three input features ($MS_s^i, PAN_s^i, Fu^i \in \mathbb{R}^{B \times L \times D}$), firstly, MS_s^i and PAN_s^i is fused, and then the result is fused with Fu^i . In the following, the fusion of MS_s^i and PAN_s^i is taken as an example.

This paper concatenates them along the dimensions of D . The concatenated result is then processed by a linear mapping layer to obtain a pixel-by-pixel attention coefficient matrix $G \in \mathbb{R}^{B \times L \times D}$, where L is the number of tokens and D is the number of features in each token (the volume of tokens):

$$G = \text{Linear}([MS_s^i, PAN_s^i]). \quad (18)$$

(2) Fusion feature extraction. After obtaining the attention coefficient matrix, it is entered into the linear fusion module (LFM) together with the two input modal features to obtain the fusion result $Fu \in \mathbb{R}^{B \times L \times D}$. Specifically, in the LFM, taking the calculation of Fu_{ld} as an example (Fu_{ld} representing the eigenvalue of the d th position of the l th token in the fused feature Fu). First, MS_{sl}^i is multiplied by the entire token of PAN_{sl}^i . It can be understood as the influence of the fusion of PAN_{sl}^i on MS_{sl}^i . Then, the above results are multiplied by the coefficient values G_{ld} of the corresponding position in the attention coefficient matrix to obtain the fusion matrix Fu_{ld}^* of this position. Finally, the fusion value Fu_{ld} of the position is obtained by applying the global average pooling to Fu_{ld}^* . Similarly, the pixel-by-pixel linear fusion operation of the two

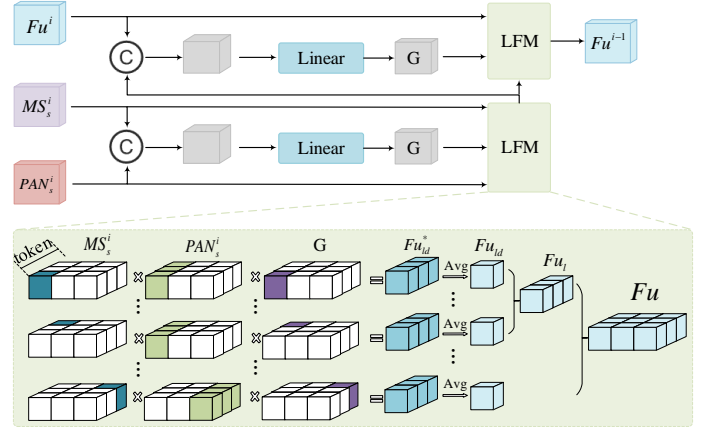


Fig. 5: Attention-Aware Linear Fusion Module (AALF-Module). LFM is linear fusion operation. G represents the pixel-by-pixel attention coefficient matrix generated by the fused features.

modals can obtain the fusion feature $Fu \in \mathbb{R}^{B \times L \times D}$. The specific process is as follows:

$$Fu = \text{LFM}(MS_s^i, PAN_s^i, G), \quad (19)$$

$$Fu_{ld} = \text{GAP}(MS_{sl}^i \times PAN_{sl}^i \times G_{ld}). \quad (20)$$

Among them, $\text{GAP}(\cdot)$ represents the global average pooling operation.

The AALF-Module performs pixel-wise fusion guided by computed influence coefficients. So, it can show good results when fusing features with large semantic differences, which greatly improves the utilization of multimodal image and the generalization ability of models.

Algorithm 1 DAS²F-Model

Require: MS : the MS image; PAN : the PAN image; y : the ground-truth of MS image;
Ensure: P_{model} : trained model;
1: epoch = 0;
2: **while** epoch < max_epoch **do**
3: $MS_p = \text{PreMs}(MS)$ (Eq. (4));
4: $PAN_p = \text{PrePAN}(PAN)$ (Eq. (4));
5: **while** i < N **do**
6: $MS_c^i, MS_s^i, PAN_c^i, PAN_s^i =$
 CMDAⁱ(MS_c^{i-1}, PAN_c^{i-1}) (Sec. III-C);
7: **end while**
8: $Fu^n = (MS_c^n + PAN_c^n)/2$ (Eq. (7));
9: **while** i < N **do**
10: $Fu^{i-1} = \text{AALF}(Fu^i, MS_s^i, PAN_s^i)$ (Sec. III-D);
11: **end while**
12: $L = -\frac{1}{N} \sum_{i=1}^N \sum_{j=1}^C y_{ij} \log(\text{MLP}(Fu))_{ij}$ (Eq. (8));
13: epoch = epoch + 1;
14: **end while**

The DAS²F-Model (pseudocode provided in Algorithm 1) separates the common essential features and their respective dominant features of multimodal image by the CMDA-

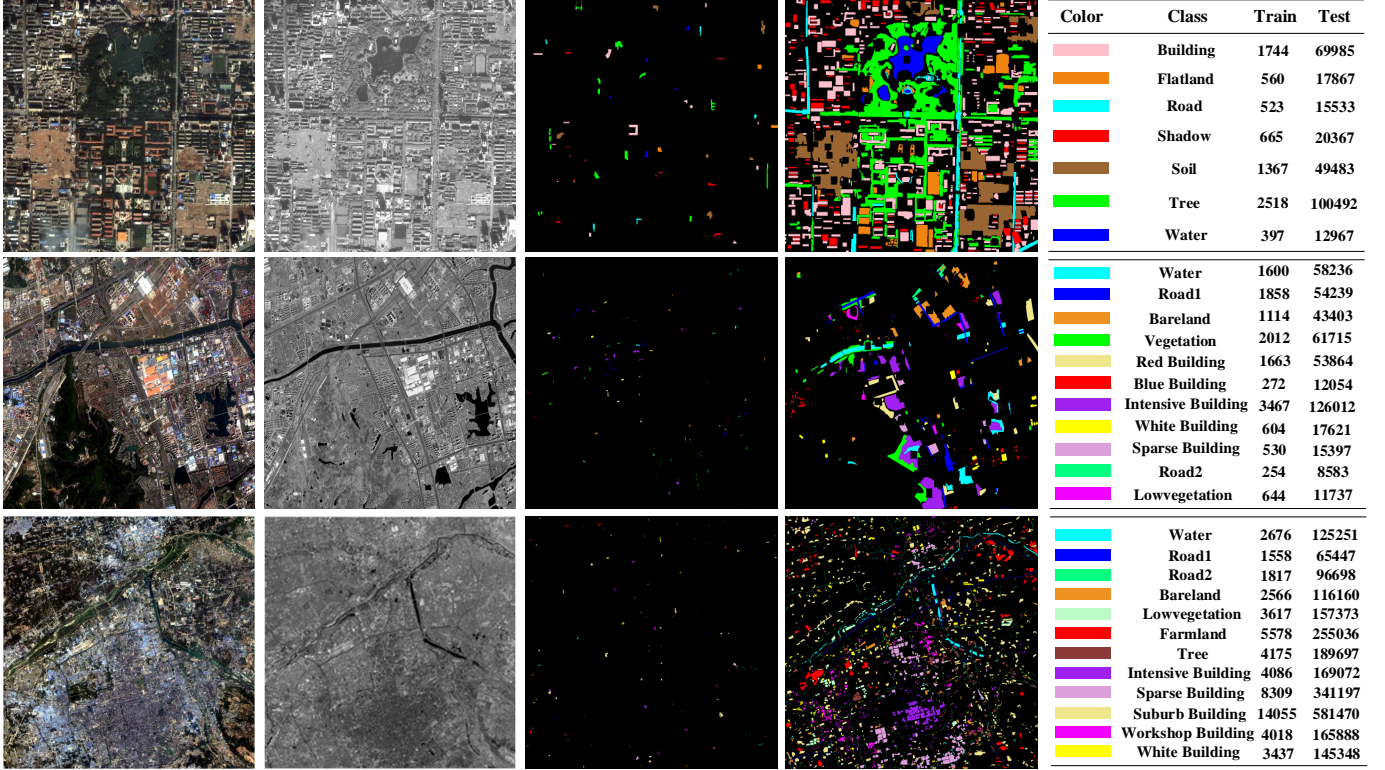


Fig. 6: Visualization of datasets. From top to bottom are the scenes of Xi'an Urban, Nanjing and Xi'an. From left to right are MS images, PAN images, training sets, test sets, and related data statistics.

Module. Among this, the SPVM extracts both local and global features of the input image. Moreover, the AALF-Module is used to fuse them to further improve the classification performance and generalization ability of the model.

IV. EXPERIMENTAL STUDY

This section systematically evaluates the DAS²F-Model's performance through four key aspects: datasets and equipment specifications, hyperparameter selection, ablation experiment, and comparative analysis with existing methods.

A. Datasets Description and Experimental Settings

1) *Datasets*: This paper utilizes three paired multispectral and panchromatic datasets (Fig. 6), which are obtained from the Key Laboratory of Intelligent Perception and Image Understanding under the Ministry of Education. The datasets are described in detail below:

(1) Xi'an urban : The MS image is characterized by dimensions of 800×830 pixels, encompassing four spectral bands with an 8m resolution. Conversely, the PAN image exhibits dimensions of 2400×2520 pixels and consists of a single-channel spectral band with a finer 2m resolution. Within the dataset, labels have been provided for seven distinct types of ground scenes, totaling 294468 samples. Notably, 7774 samples are earmarked for training purposes, leaving a substantial 286694 samples for subsequent testing and evaluation.

(2) Xi'an : The MS image is a color image with a spatial resolution of 8 m and dimensions of $4548 \times 4541 \times 4$ pixels. The

PAN image has a grayscale resolution of $18192 \times 18164 \times 1$ pixels with a spatial resolution of 2 m. The collection includes labels for twelve different categories of ground scenes, totaling 2364529 samples. Notably, 55892 samples are set aside for training, leaving a significant 2408637 samples for later testing and evaluation.

(3) Nanjing : The dataset provides the MS image measuring 2000×2500 pixels and containing four spectral bands at an 8m resolution. In comparison, there is the PAN image with dimensions of 8000×10000 pixels and a single-channel spectral band with a better 2m resolution. The dataset contains labels representing eleven different ground scene classes, for a total of 476879 samples. It is worth noting that 14018 samples are set aside for training, while the remaining 462863 samples are kept for future testing and evaluation.

2) *Experimental settings*: The experiments conducted in this study were performed on a computing platform equipped with an RTX2080Ti GPU (12 GB memory) and 128 GB RAM. The network is trained through the use of the PyTorch framework. Throughout the training phase, the weight decay is established at 0.0005, with the number of epochs set to 25 and the initial learning rate for the Xi'an dataset is 0.000393, while the other two datasets use a learning rate of 0.000293. For the Nanjing and Xi'an datasets, a batch size of 128 is implemented, whereas the Xi'an urban datasets are trained using a batch size of 64.

3) *Quality Evaluation Indicators*: Our experimental protocol incorporates a multi-dimensional evaluation framework to rigorously assess model performance. The assessment method-

TABLE I: EXPERIMENTAL RESULT OF THE DAS²F-Model HYPERPARAMETER BLOCK NUMBERS N

| Dataset | Xi'an Urban | | | | Nanjing | | | | Xi'an | | | |
|---------|--------------|-------|-------|-------|---------|--------------|-------|-------|-------|-------|--------------|-------|
| | [1,1] | [2,2] | [3,3] | [4,4] | [1,1] | [2,2] | [3,3] | [4,4] | [1,1] | [2,2] | [3,3] | [4,4] |
| N | | | | | | | | | | | | |
| OA | 85.35 | 83.91 | 83.38 | 82.41 | 77.35 | 79.11 | 76.32 | 74.29 | 80.50 | 80.38 | 80.56 | 79.29 |
| AA | 79.20 | 77.65 | 73.35 | 75.72 | 73.72 | 73.92 | 71.87 | 69.90 | 73.90 | 73.63 | 73.93 | 72.13 |
| Kappa | 81.14 | 79.33 | 78.39 | 77.39 | 73.70 | 75.54 | 72.40 | 70.09 | 77.69 | 77.54 | 77.74 | 76.31 |

TABLE II: RESULTS OF THE ABLATION STUDY ON THE XIAN URBAN IMAGE

| | Visual Mamba | CMDA | SPVM | AALF | OA(%) | AA(%) | Kappa(%) |
|-----|--------------|------|------|------|--------------|--------------|--------------|
| (1) | ✓ | | | | 79.02 | 71.01 | 72.92 |
| (2) | ✓ | | | ✓ | 82.25 | 75.30 | 77.23 |
| (3) | ✓ | ✓ | | | 80.81 | 72.62 | 75.25 |
| (4) | ✓ | ✓ | | ✓ | 83.77 | 76.48 | 79.01 |
| (5) | ✓ | ✓ | ✓ | ✓ | 85.35 | 79.20 | 81.14 |

ology examines three principal metrics: overall accuracy (OA) serves as the primary indicator of global prediction correctness across all classes; average accuracy (AA) provides insights into potential classification bias by evaluating mean performance distribution among categories; Kappa coefficient statistic (Kappa) offers a chance-corrected agreement measurement that accounts for random prediction effects, delivering more statistically robust performance interpretation. This comprehensive metric system ensures thorough validation of the generalization capacity and operational stability of the DAS²F-Model under diverse conditions.

B. Selection of Hyperparameters

Since the feature separation and fusion operations exhibit a one-to-one correspondence, the number of CMDA-Module and AALF-Module should remain consistent, denoted as N. In order to explore the influence of N on the DAS²F-Model, we set N to 1, 2, 3, 4 to compare the accuracy versus parameters of the three datasets.

The results are shown in Tables I. On the datasets of Xi'an Urban, Nanjing and Xi'an, the network attains the best accuracy when N is 1, 2 and 3, respectively. This is because datasets of varying sizes require different numbers of modules to effectively separate the common and dominant features across the two modalities. For the smallest Xi'an Urban dataset, only one CMDA-Module is needed to complete the separation of common features and dominant features. However, for the largest Xi'an dataset, three CMDA-Module are needed to complete. In each data set, when the value of N exceeds the optimal threshold, the performance of the model will be decreased, because when N is equal to the optimal threshold, the common features and the dominant features are separated, and the subsequent excessive modules produce more redundant features in the dominant features, resulting in the failure of the feature separation module, and then the performance of the model will be reduced.

C. Ablation Experiment

In this paper, we have randomly chosen the Xi'an Urban dataset for a comprehensive combinatorial investigation involving space preserving visual mamba (SPVM), cross-modal diff-attention module (CMDA-Module), as well as attention-aware linear fusion module (AALF-Module). By conducting experiments with various combinations of these modules, we aim to assess their individual effectiveness and necessity within the network architecture. The detailed results of these experiments are meticulously documented in Table II, providing insights into the impact and significance of each module in optimizing network performance on the Xi'an Urban dataset.

In the experimental verification on the Xi'an Urban dataset, the DAS²F-Model achieves the best performance (OA: 85.35%, AA: 79.20%, Kappa: 81.14%) through the close collaboration of its three core modules (SPVM \cup CMDA-Module \cup AALF-Module). This is because the SPVM can extract global features of the image while combining convolutional neural network to compensate for local features, and can also capture the local context relationship between independent tokens. The CMDA-Module can effectively separate the common and dominant features of multimodal data by exchanging the intermediate matrix generated in the state space model, thereby reducing the feature redundancy in the fusion stage. In addition, the AALF-Module can effectively fuse features with large semantic differences while keeping the feature size constant. The integrated solution works together on the DAS²F-Model, which makes it perform well in handling multisource remote sensing image classification.

D. Experiment Results and Comparison Algorithms

In Xi'an Urban, Nanjing and Xi'an dataset, the proposed DAS²F-Model is compared with seven state-of-the-art methods, namely CRHFF [38], AM³Net [41], GCFNet [42], MFT [34], DFNet [39], NNCNet [40] and ISSP [28]. Tables III, IV and V show the results of the quantitative comparison experiments, respectively, and Figs. 7, 8 and 9 show the visualizations of the comparison algorithms, respectively.

1) Experiment Results and Analysis on Xi'an Urban Area:

The CRHFF [38] utilizes integrated shallow-to-deep features combined with global-to-local characteristics from high-resolution MS and PAN images. By extracting and fusing cross-resolution information, it enhances multimodal representation modeling, leading to improved classification accuracy. It achieves high accuracy on c_5 (Soil: 90.99%) and c_7 (Water: 98.04%) categories.

The AM³Net [41] can measure the contribution rate of each pixel's spectral channel to the construction of spectral feature tensor independently, and realize the cooperative transmission

TABLE III:
QUANTITATIVE RESULTS OF THE Xi'an Urban DATASET

| Models | CRHFF [38] | AM ³ Net [41] | GCFNet [42] | MFT [34] | DFINet [39] | NNCNet [40] | ISSP [28] | DAS ² F-Model |
|------------------|------------|--------------------------|-------------|----------|--------------|--------------|--------------|--------------------------|
| c_1 : Building | 77.53 | 84.27 | 72.96 | 74.96 | 71.58 | 85.62 | 76.39 | 84.23 |
| c_2 : Flatland | 40.93 | 35.89 | 30.75 | 46.82 | 52.87 | 38.35 | 37.21 | 36.77 |
| c_3 : Road | 73.86 | 39.09 | 25.46 | 43.74 | 80.65 | 59.89 | 64.04 | 74.04 |
| c_4 : Shadow | 75.48 | 58.12 | 42.02 | 68.17 | 45.33 | 71.41 | 83.35 | 79.21 |
| c_5 : Soil | 90.99 | 55.32 | 80.74 | 81.70 | 92.98 | 90.42 | 89.72 | 90.76 |
| c_6 : Tree | 79.98 | 82.43 | 88.36 | 82.21 | 85.55 | 92.55 | 83.22 | 93.78 |
| c_7 : Water | 98.04 | 96.86 | 71.37 | 98.09 | 98.71 | 95.61 | 97.89 | 98.58 |
| OA(%) | 79.01 | 71.87 | 72.23 | 75.78 | 78.86 | 83.98 | 79.44 | 85.35 |
| AA(%) | 76.69 | 64.57 | 58.81 | 70.81 | 75.38 | 76.26 | 75.97 | 79.20 |
| Kappa(%) | 73.35 | 63.19 | 63.97 | 68.89 | 72.82 | 79.31 | 73.80 | 81.14 |

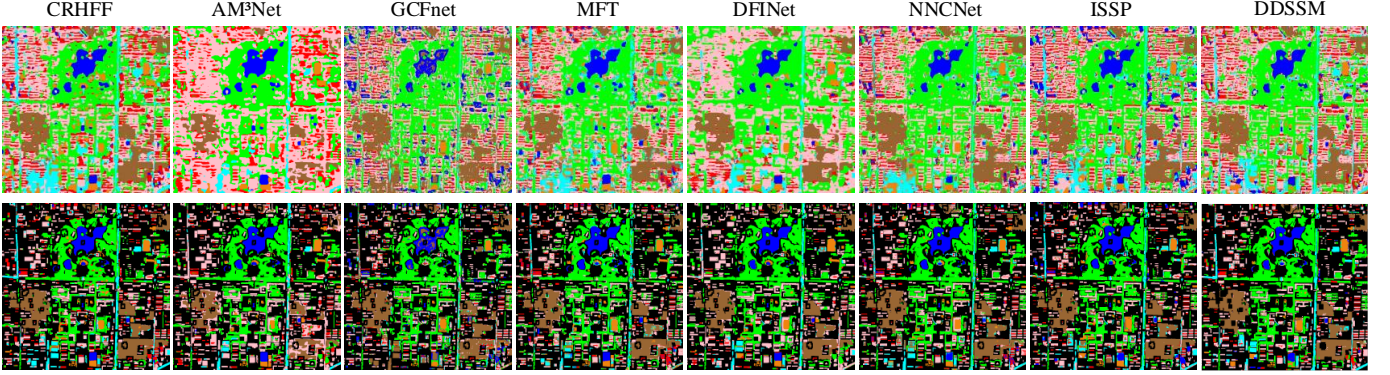


Fig. 7: Visualization results of experimental on Xi'an Urban. Each column contains an overall color map and a label position color map. From left to right, they are CRHFF, AM³Net, GCFNet, MFT, DFINet, NNCNet, ISSP, DAS²F-Model.

of spectral features and spatial information through a spectral spatial mutual conduction module. It demonstrates higher accuracy on c_1 (Building: 84.27%) category.

The GCFNet [42] is an encoder-decoder based global cooperative fusion network, which improves performance by exploiting the context dependency and fusing sampled and unsampled location data. Additionally, an adaptive loss weighted fusion strategy is designed to calculate the total loss of two individual and cross-modal branches. Compared with AM³Net, it has attained a large improvement on c_5 (Soil: 80.74% vs 55.32%) category.

The MFT [34] improves the generalization ability of the model by utilizing a multihead cross-patch attention and additional supplementary information sources. At the same time, the concept of tokenization is introduced to learn a distinctive representation in a reduced and hierarchical feature space, thereby improving the HSI land cover classification performance. Although it does not have the highest accuracy category, the overall accuracy is relatively average, and there is no worst category.

The DFINet [39] can extract autocorrelation and cross-correlation from multisource feature pairs, thus highlighting meaningful complementary information for classification. At the same time, the consistency loss, discrimination loss and classification loss are coordinated to improve the classification accuracy. Therefore, it achieves the highest category accuracy on c_2 (Flatland: 52.87%), c_3 (Road: 80.65%), c_5 (Soil: 92.98%) and c_7 (Water: 98.71%) categories. However, it performs too poorly on the other categories, resulting in a

low AA (75.38%).

The NNCNet [40] uses unlabeled data through self-supervised learning to overcome the problem of inconsistent distribution of multisource data. It uses nearest neighbor data enhancement and bilinear attention modules to enhance semantic similarity and feature interaction respectively, improving classification results. It demonstrates the highest category accuracy on c_1 (Building: 85.62%) category.

The ISSP [28] addresses the problem of effectively utilizing complementary information from PAN and MS images by using pixel-guided spatial enhancement and time-frequency cooperative spectral enhancement. It attains the highest category accuracy on c_4 (Shadow: 83.35%) category.

The DAS²F-Model captures de-redundant global long-range dependencies with linear complexity. The SPVM can simultaneously capture the global and local features of the image, and can model the local context relationship between independent tokens. The CMDA-Module effectively separates the common and dominant features of MS and PAN images, thus reduces the feature redundancy in the fusion stage. The AALF-Module successfully fuses features that have large semantic differences and effectively realizes the fusion of multimodal features. Therefore, it achieves the highest classification accuracy in category c_6 (Tree: 93.78%). Moreover, the DAS²F-Model can provide a more robust and comprehensive solution, which makes it better than those models that only focus on a single feature extraction method in terms of comprehensive performance. That is, the DAS²F-Model overall OA (85.35%), AA (79.20%), and kappa (81.14%) are the highest.

TABLE IV:
QUANTITATIVE RESULTS OF THE Nanjing DATASET

| Models | CRHFF [38] | AM ³ Net [41] | GCFNet [42] | MFT [34] | DFINet [39] | NNCNet [40] | ISSP [28] | DAS ² F-Model |
|----------------------------|--------------|--------------------------|-------------|----------|--------------|--------------|--------------|--------------------------|
| c_1 : Water | 94.86 | 88.44 | 93.45 | 94.23 | 96.18 | 94.77 | 94.24 | 96.02 |
| c_2 : Road1 | 72.96 | 40.62 | 37.36 | 64.21 | 72.09 | 67.25 | 59.47 | 67.73 |
| c_3 : Bareland | 94.24 | 54.10 | 84.98 | 91.84 | 92.23 | 88.19 | 94.50 | 93.95 |
| c_4 : Vegetation | 84.85 | 71.55 | 78.65 | 76.58 | 88.77 | 75.83 | 80.80 | 79.93 |
| c_5 : Red Building | 77.61 | 67.85 | 24.98 | 75.54 | 85.50 | 77.94 | 78.04 | 79.95 |
| c_6 : Blue Building | 95.59 | 93.66 | 44.95 | 91.60 | 97.09 | 93.03 | 75.33 | 95.32 |
| c_7 : Intensive Building | 59.08 | 74.96 | 64.42 | 64.48 | 64.35 | 75.72 | 69.34 | 77.07 |
| c_8 : White Building | 81.76 | 90.98 | 64.74 | 75.73 | 86.71 | 84.37 | 58.44 | 85.44 |
| c_9 : Sparse Building | 53.61 | 80.99 | 45.62 | 38.92 | 44.81 | 47.68 | 52.80 | 44.50 |
| c_{10} : Road2 | 43.07 | 91.86 | 13.58 | 34.21 | 30.92 | 53.03 | 33.90 | 34.57 |
| c_{11} : Lowvegetation | 62.74 | 43.96 | 47.84 | 63.27 | 63.27 | 66.78 | 59.09 | 58.64 |
| OA(%) | 75.52 | 70.22 | 61.65 | 73.35 | 78.00 | 77.77 | 75.01 | 79.11 |
| AA(%) | 74.85 | 72.63 | 54.60 | 70.06 | 74.72 | 74.96 | 70.54 | 73.92 |
| Kappa(%) | 71.77 | 65.02 | 55.01 | 69.11 | 74.47 | 74.03 | 71.03 | 75.54 |

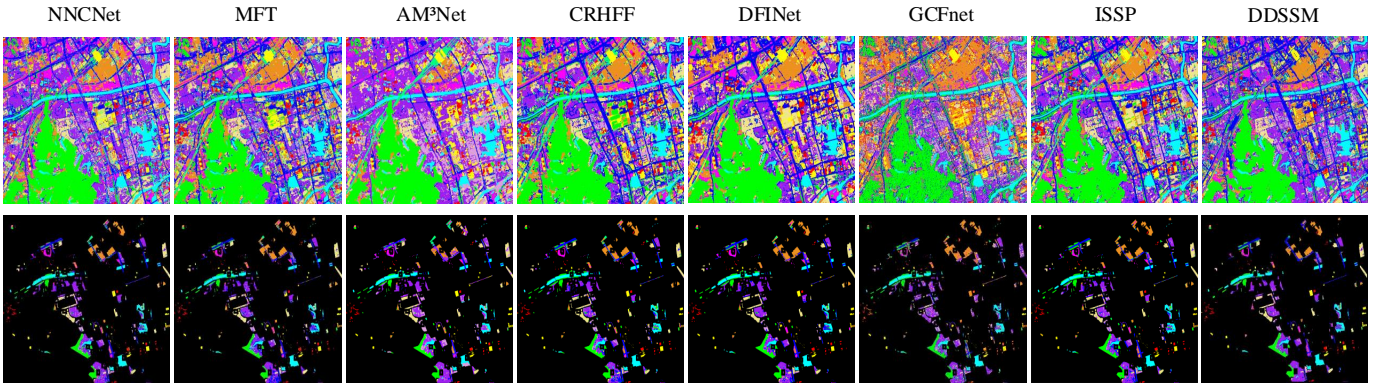


Fig. 8: Visualization results of experimental on Nanjing. Each column contains an overall color map and a label position color map. From left to right, they are CRHFF, AM³Net, GCFNet, MFT, DFINet, NNCNet, ISSP, DAS²F-Model.

2) Experiment Results and Analysis on Nanjing Area:

The DAS²F-Model leverages exceptional feature interaction capabilities, leading to optimal classification accuracy in c_7 (Intensive Building: 77.07%). Notably, it also demonstrates superior performance with an OA of 79.11%, AA of 73.92%, and Kappa coefficient of 75.54%. The CRHFF utilizes an encoder to extract multi-channel and high-resolution features, excelling in global background feature extraction and yielding impressive results in c_2 (Road1: 72.96%). The spatial location capturing ability of AM³Net contributes to excellent categorization in c_8 (White Building: 90.98%), c_9 (Sparse Building: 80.99%) and c_{10} (Road2: 91.86%). The DFINet exhibits spectral collection capabilities, reflecting superior performance in c_1 (Water: 96.18%), c_4 (Vegetation: 88.77%), c_5 (Red Building: 85.50%) and c_6 (Blue Building: 97.09%). The NNCNet enhances neighborhood information using a bilinear attention module, achieving peak accuracy in category c_{11} (Low vegetation: 66.78%). The ISSP effectively integrates multi-scale context information while emphasizing pixel-level features, achieves the highest accuracy in category c_3 (Bareland: 94.50%).

3) Experiment Results and Analysis on Xi'an Area:

By comparing the performance of different models, it can be seen that the DAS²F-Model performs best in overall performance indicators, with OA, AA, and Kappa of 80.56%, 73.93%, and 77.74% respectively, all higher than other models.

Specifically for each category, the performance of each model in different categories is different. For example, the MFT excels in c_1 (Water: 97.35%) category, while the NNCNet demonstrates superior performance in c_2 (Road1: 34.16%). In other categories, the AM³Net demonstrates the highest accuracy in c_6 (Farmland: 76.35%), c_9 (Sparse Building: 80.85%) and c_{10} (Suburb Building: 99.81%) categories, benefiting from its involution operator. Leveraging deep cross-attention mechanisms, the DFINet attains superior performance in c_4 (Bareland: 75.55%), c_7 (Tree: 92.29), c_8 (Intensive Building: 86.75%) and c_{12} (White Building: 83.25%). Meanwhile, the CRHFF and the ISSP demonstrate superior performance in c_5 (Lowvegetation: 55.51%), c_{11} (Workshop Building: 95.39%) and c_3 (Road2: 68.75%), respectively. Although the DAS²F-Model does not achieve the highest accuracy in any specific category, it consistently maintains competitive performance across all classes. This suggests that our approach maintains robust classification capability across all categories rather than excelling in specific classes at the expense of others. These results further prove that the overall classification performance of the DAS²F-Model on the Xi'an dataset is better than other models, and has better generalization ability and robustness.

Quantitative assessments reveal that the DAS²F-Model surpasses most reference algorithms in classification accuracy, with rigorous testing across multiple datasets confirming its state-of-the-art performance metrics.

TABLE V:
QUANTITATIVE RESULTS OF THE Xi'an DATASET

| Models | CRHFF [38] | AM ³ Net [41] | GCFNet [42] | MFT [34] | DFINet [39] | NNCNet [40] | ISSP [28] | DAS ² F-Model |
|------------------------------|--------------|--------------------------|-------------|--------------|--------------|--------------|--------------|--------------------------|
| c_1 : Water | 95.89 | 95.61 | 95.89 | 97.35 | 93.51 | 93.15 | 96.75 | 96.62 |
| c_2 : Road1 | 18.35 | 1.72 | 17.46 | 16.82 | 15.41 | 34.16 | 26.29 | 22.26 |
| c_3 : Road2 | 62.01 | 11.61 | 55.38 | 50.69 | 53.66 | 62.14 | 68.75 | 62.95 |
| c_4 : Bareland | 66.45 | 67.74 | 66.46 | 64.58 | 75.55 | 69.01 | 72.70 | 69.47 |
| c_5 : Lowvegetation | 55.51 | 18.81 | 36.06 | 46.68 | 45.00 | 55.10 | 54.81 | 45.02 |
| c_6 : Farmland | 69.74 | 76.35 | 64.31 | 51.69 | 50.59 | 68.41 | 71.42 | 73.43 |
| c_7 : Tree | 84.84 | 37.73 | 89.12 | 91.78 | 92.29 | 77.92 | 86.47 | 90.44 |
| c_8 : Intensive Building | 77.59 | 72.44 | 72.65 | 62.85 | 86.75 | 74.62 | 74.57 | 83.43 |
| c_9 : Sparse Building | 77.18 | 80.85 | 76.40 | 75.73 | 78.26 | 77.48 | 77.17 | 75.59 |
| c_{10} : Suburb Building | 95.51 | 99.81 | 97.81 | 91.90 | 96.06 | 96.81 | 95.47 | 97.67 |
| c_{11} : Workshop Building | 95.39 | 75.48 | 90.71 | 94.52 | 96.75 | 94.23 | 92.03 | 93.79 |
| c_{12} : White Building | 75.33 | 45.00 | 66.36 | 72.87 | 83.25 | 76.02 | 67.29 | 76.43 |
| OA(%) | 79.42 | 69.58 | 76.86 | 74.65 | 78.70 | 79.24 | 79.58 | 80.56 |
| AA(%) | 72.81 | 56.93 | 69.05 | 68.12 | 72.26 | 73.25 | 73.64 | 73.93 |
| Kappa(%) | 76.44 | 64.18 | 73.48 | 71.08 | 75.78 | 76.24 | 76.66 | 77.74 |

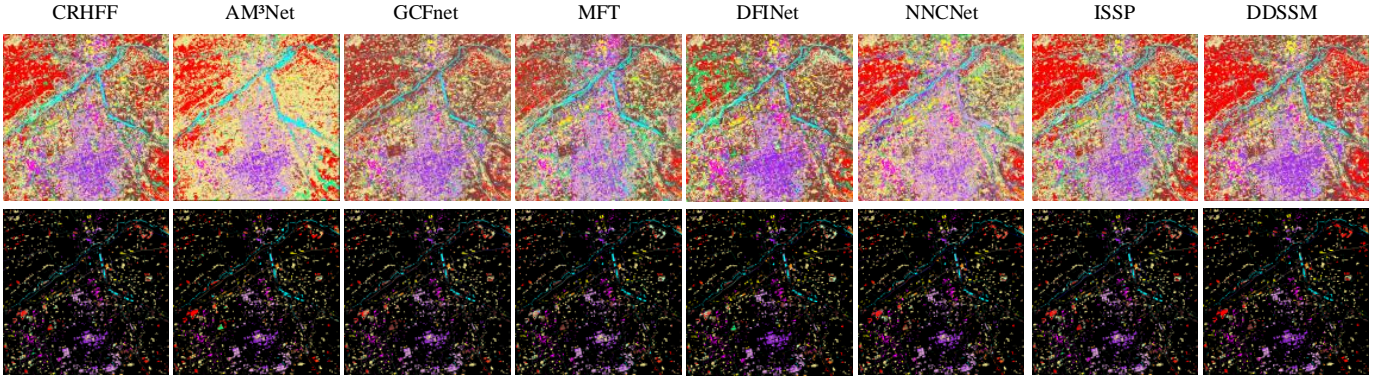


Fig. 9: Visualization results of experimental on Xi'an. Each column contains an overall color map and a label position color map. From left to right, they are CRHFF, AM³Net, GCFNet, MFT, DFINet, NNCNet, ISSP, DAS²F-Model.

V. CONCLUSION

In this paper, a diff-attention aware state space fusion model (DAS²F-Model) is proposed. It mainly includes the cross-modal diff-attention module (CMDA-Module) and the attention-aware linear fusion module (AALF-Module). The CMDA-Module uses diff-attention mechanism to effectively separate the common features and dominant features of MS and PAN images, reducing the redundancy of the feature fusion stage. At the same time, space preserving visual mamb (SPVM) is used to capture the global and local features of the image, and the global context relationship between independent tokens is modeled. The AALF-Module effectively fuse features with large semantic differences while keeping the size of fusion features unchanged by calculating the overall pixel-by-pixel influence of one modality on the other modality. The effectiveness and robustness of the DAS²F-Model is demonstrated through experiments on three datasets. Future research will focus on enhancing the model's generalization capabilities while maintaining its current level of precision, particularly for deployment in more diverse real-world scenarios.

REFERENCES

- [1] Jian Long, Yibing Zhan, Zhengbin Pang, Tong Zhou, Xueqiong Li, Long Lan, and Yuanxi Peng. Joint spatial-spectral optimization for the high-magnification fusion of hyperspectral and multispectral images. *IEEE Transactions on Geoscience and Remote Sensing*, 62:1–19, 2024.
- [2] Xueli Geng, Licheng Jiao, Lingling Li, F. Liu, Xu Liu, Shuyuan Yang, and Xiangrong Zhang. Multisource joint representation learning fusion classification for remote sensing images. *IEEE Transactions on Geoscience and Remote Sensing*, 61:1–14, 2023.
- [3] Leo Thomas Ramos and Angel D. Sappa. Multispectral semantic segmentation for land cover classification: An overview. *IEEE Journal of Selected Topics in Applied Earth Observations and Remote Sensing*, 17:14295–14336, 2024.
- [4] Mengru Ma, Wenping Ma, Licheng Jiao, Xu Liu, Fang Liu, Lingling Li, and Shuyuan Yang. Mbsi-net: Multimodal balanced self-learning interaction network for image classification. *IEEE Trans. Cir. and Sys. for Video Technol.*, 34(5):3819–3833, May 2024.
- [5] Guangxu Xie, Ren qi Nie, Jinde Cao, He Li, and Jintao Li. A deep multiresolution representation framework for pansharpening. *IEEE Transactions on Geoscience and Remote Sensing*, 62:1–16, 2024.
- [6] Rui Sun, Feng Zhao, Chengquan Huang, Huabing Huang, Zhong Lu, Ping Zhao, Xiang Ni, and Ran Meng. Integration of deep learning algorithms with a bayesian method for improved characterization of tropical deforestation frontiers using sentinel-1 sar imagery. *Remote Sensing of Environment*, 2023.
- [7] Gang Chen, Yuyu Zhou, James A. Voigt, and Eleanor C. Stokes. Remote sensing of diverse urban environments: From the single city to multiple cities. *Remote Sensing of Environment*, 305:114108, 2024.
- [8] Danfeng Hong, Bing Zhang, Hao Li, Yuxuan Li, Jing Yao, Chenyu Li, Martin Werner, Jocelyn Chanussot, Alexander Zipf, and Xiao Xiang Zhu. Cross-city matters: A multimodal remote sensing benchmark dataset for cross-city semantic segmentation using high-resolution domain adaptation networks. *Remote Sensing of Environment*, 299:113856, 2023.
- [9] Changhong Xu, Maofang Gao, Jingwen Yan, Yunxiang Jin, Guijun Yang, and Wenbin Wu. Mp-net: An efficient and precise multi-layer pyramid crop classification network for remote sensing images. *Computers and Electronics in Agriculture*, 212:108065, 2023.
- [10] Shunping Ji, Dingpan Wang, and Muying Luo. Generative adversarial network-based full-space domain adaptation for land cover classification

- from multiple-source remote sensing images. *IEEE Transactions on Geoscience and Remote Sensing*, 59(5):3816–3828, 2021.
- [11] Xin Wu, Danfeng Hong, and Jocelyn Chanussot. Convolutional neural networks for multimodal remote sensing data classification. *IEEE Transactions on Geoscience and Remote Sensing*, 60:1–10, 2022.
 - [12] Hojat Shirmard, Ehsan Farahbakhsh, R. Dietmar Müller, and Rohitash Chandra. A review of machine learning in processing remote sensing data for mineral exploration. *Remote Sensing of Environment*, 268:112750, 2022.
 - [13] Qingfa Meng, Guoqing Ma, Lili Li, Taihan Wang, Zongrui Li, Nan Wang, and Jingyu Li. Joint inversion of gravity and magnetic data with tetrahedral unstructured grid and its application to mineral exploration. *IEEE Transactions on Geoscience and Remote Sensing*, 61:1–14, 2023.
 - [14] Xingqian Du, Xiangtao Zheng, Xiaoqiang Lu, and Alexander A. Doudkin. Multisource remote sensing data classification with graph fusion network. *IEEE Transactions on Geoscience and Remote Sensing*, 59(12):10062–10072, 2021.
 - [15] Wenping Ma, Jianchao Shen, Hao Zhu, Jun Zhang, Jiliang Zhao, Biao Hou, and Licheng Jiao. A novel adaptive hybrid fusion network for multiresolution remote sensing images classification. *IEEE Transactions on Geoscience and Remote Sensing*, 60:1–17, 2022.
 - [16] Hao Zhu, Kenan Sun, Licheng Jiao, Xiaotong Li, Fang Liu, Biao Hou, and Shuang Wang. Adaptive dual-path collaborative learning for pan and ms classification. *IEEE Transactions on Geoscience and Remote Sensing*, 60:1–15, 2022.
 - [17] Xiaotong Li, Licheng Jiao, Hao Zhu, Fang Liu, Shuyuan Yang, Xiangrong Zhang, Shuang Wang, and Rong Qu. A collaborative learning tracking network for remote sensing videos. *IEEE Transactions on Cybernetics*, 53(3):1954–1967, 2023.
 - [18] Gemine Vivone, Mauro Dalla Mura, Andrea Garzelli, Rocco Restaino, Giuseppe Scarpa, Magnus O. Ulfarsson, Luciano Alparone, and Jocelyn Chanussot. A new benchmark based on recent advances in multispectral pansharpening: Revisiting pansharpening with classical and emerging pansharpening methods. *IEEE Geoscience and Remote Sensing Magazine*, 9(1):53–81, 2021.
 - [19] Xiangchao Meng, Huanfeng Shen, Huifang Li, Liangpei Zhang, and Randi Fu. Review of the pansharpening methods for remote sensing images based on the idea of meta-analysis: Practical discussion and challenges. *Inf. Fusion*, 46:102–113, 2019.
 - [20] Gemine Vivone, Luciano Alparone, Andrea Garzelli, and Simone Lolli. Fast reproducible pansharpening based on instrument and acquisition modeling: Awlp revisited. *Remote. Sens.*, 11:2315, 2019.
 - [21] Bruno Aiazzi, Stefano Baronti, and Massimo Selva. Improving component substitution pansharpening through multivariate regression of ms + pan data. *IEEE Transactions on Geoscience and Remote Sensing*, 45(10):3230–3239, 2007.
 - [22] P. Mangalraj, V. Sivakumar, S. Karthick, V. Haribaabu, S. Ramraj, and Dinesh Jackson Samuel. A review of multi-resolution analysis (mra) and multi-geometric analysis (mga) tools used in the fusion of remote sensing images. *Circuits, Systems, and Signal Processing*, 39(6):1–28, 2019.
 - [23] Sen Jia, Kuilin Wu, Jiasong Zhu, and Xiuping Jia. Spectral-spatial gabor surface feature fusion approach for hyperspectral imagery classification. *IEEE Transactions on Geoscience and Remote Sensing*, 57(2):1142–1154, 2019.
 - [24] Ihnen Hedhli, Gabriele Moser, Sebastiano B. Serpico, and Josiane Zerubia. Classification of multisensor and multiresolution remote sensing images through hierarchical markov random fields. *IEEE Geoscience and Remote Sensing Letters*, 14(12):2448–2452, 2017.
 - [25] Jiaxuan Zhao, Licheng Jiao, Chao Wang, Xu Liu, Fang Liu, Lingling Li, Mengru Ma, and Shuyuan Yang. Knowledge guided evolutionary transformer for remote sensing scene classification. *IEEE Transactions on Circuits and Systems for Video Technology*, 34(10):10368–10384, 2024.
 - [26] Licheng Jiao, Xin Zhang, Xu Liu, Fang Liu, Shuyuan Yang, Wenping Ma, Lingling Li, Puhua Chen, Zhixi Feng, Yuwei Guo, Xu Tang, Biao Hou, Xiangrong Zhang, Jing Bai, Dou Quan, and Junpeng Zhang. Transformer meets remote sensing video detection and tracking: A comprehensive survey. *IEEE Journal of Selected Topics in Applied Earth Observations and Remote Sensing*, 16:1–45, 2023.
 - [27] Yilin Shao, Long Sun, Licheng Jiao, Xu Liu, Fang Liu, Lingling Li, and Shuyuan Yang. Cot: Contourlet transformer for hierarchical semantic segmentation. *IEEE Transactions on Neural Networks and Learning Systems*, 36(1):132–146, 2025.
 - [28] Wenping Ma, Hekai Zhang, Mengru Ma, Chuang Chen, and Biao Hou. Issp-net: An interactive spatial-spectral perception network for multimodal classification. *IEEE Transactions on Geoscience and Remote Sensing*, 62:1–14, 2024.
 - [29] Ting Lu, Kexin Ding, Wei Fu, Shutao Li, and Anjing Guo. Coupled adversarial learning for fusion classification of hyperspectral and lidar data. *Information Fusion*, 93:118–131, 2023.
 - [30] Hao Zhu, Xiaoyu Yi, Xiaotong Li, Biao Hou, Changzhe Jiao, Wenping Ma, and Licheng Jiao. Convgru-based multiscale frequency fusion network for pan-ms joint classification. *IEEE Transactions on Geoscience and Remote Sensing*, 62:1–15, 2024.
 - [31] Shenshen Zhao, Haiyong Chen, Chuhan Wang, and Shijie Shi. Sncf-net: Scale-aware neighborhood correlation feature network for hotspot defect detection of photovoltaic farms. *Measurement*, 206:112342, 2023.
 - [32] Hao Zhu, Mengru Ma, Wenping Ma, Licheng Jiao, Shikuan Hong, Jianchao Shen, and Biao Hou. A spatial-channel progressive fusion resnet for remote sensing classification. *Information Fusion*, 70:72–87, 2021.
 - [33] Lin Xu, Hao Zhu, Licheng Jiao, Wenhao Zhao, Xiaotong Li, Biao Hou, Zhongle Ren, and Wenping Ma. A dual-stream transformer with diff-attention for multispectral and panchromatic classification. *IEEE Transactions on Geoscience and Remote Sensing*, 61:1–14, 2023.
 - [34] Swalpa Kumar Roy, Ankur Deria, Danfeng Hong, Behnood Rasti, Antonio Plaza, and Jocelyn Chanussot. Multimodal fusion transformer for remote sensing image classification. *IEEE Transactions on Geoscience and Remote Sensing*, 61:1–20, 2023.
 - [35] Sheng Fang, Kaiyu Li, and Zhe Li. S²enet: Spatial-spectral cross-modal enhancement network for classification of hyperspectral and lidar data. *IEEE Geoscience and Remote Sensing Letters*, 19:1–5, 2022.
 - [36] Albert Gu and Tri Dao. Mamba: Linear-time sequence modeling with selective state spaces. *ArXiv*, abs/2312.00752, 2023.
 - [37] Mengru Ma, Jiaxuan Zhao, Wenping Ma, Licheng Jiao, Lingling Li, Xu Liu, Fang Liu, and Shuyuan Yang. A mamba-aware spatial-spectral cross-modal network for remote sensing classification. *IEEE Transactions on Geoscience and Remote Sensing*, 63:1–15, 2025.
 - [38] Sicong Liu, Hui Zhao, Qian Du, Lorenzo Bruzzone, Alim Samat, and Xiaohua Tong. Novel cross-resolution feature-level fusion for joint classification of multispectral and panchromatic remote sensing images. *IEEE Transactions on Geoscience and Remote Sensing*, 60:1–14, 2022.
 - [39] Yunhao Gao, Wei Li, Mengmeng Zhang, Jianbu Wang, Weiwei Sun, Ran Tao, and Qian Du. Hyperspectral and multispectral classification for coastal wetland using depthwise feature interaction network. *IEEE Transactions on Geoscience and Remote Sensing*, 60:1–15, 2022.
 - [40] Meng Wang, Feng Gao, Junyu Dong, Heng-Chao Li, and Qian Du. Nearest neighbor-based contrastive learning for hyperspectral and lidar data classification. *IEEE Transactions on Geoscience and Remote Sensing*, 61:1–16, 2023.
 - [41] Jinping Wang, Jun Li, Yanli Shi, Jianhuang Lai, and Xiaojun Tan. Am³net: Adaptive mutual-learning-based multimodal data fusion network. *IEEE Transactions on Circuits and Systems for Video Technology*, 32(8):5411–5426, 2022.
 - [42] Hui Zhao, Sicong Liu, Qian Du, Lorenzo Bruzzone, Yongjie Zheng, Kecheng Du, Xiaohua Tong, Huan Xie, and Xiaolong Ma. Gcfnet: Global collaborative fusion network for multispectral and panchromatic image classification. *IEEE Transactions on Geoscience and Remote Sensing*, 60:1–14, 2022.